

# Sliding Wear Studies on Heat-Treated Functionally Graded Cu–Ni–Si/TiC Composite

R. Jojith<sup>1</sup> · N. Radhika<sup>1</sup>  · U. Vipin<sup>1</sup>

Received: 7 August 2018 / Accepted: 16 November 2018 / Published online: 19 December 2018  
© The Indian Institute of Metals - IIM 2018

**Abstract** Centrifugally cast functionally graded Cu–11Ni–4Si/10 wt% TiC composite of dimension  $\text{Ø}_{\text{out}}100 \times \text{Ø}_{\text{in}}70 \times 100$  mm was heat treated to enhance the mechanical and tribological characteristics. Samples from inner zone (9–15 mm) were initially solution treated (850 °C/1 h), water quenched, and aged at varying temperatures (450, 500, and 550 °C) and ageing time (4, 6 and 8 h). The highest hardness (192 HV) displayed by the specimen aged at 550 °C/6 h was chosen for dry sliding tribological studies performed at varying applied loads (10–30 N), sliding velocities (1–3 m/s) and sliding distances (500–1500 m). An improvement of 65% was observed on comparing the micro-hardness values of heat-treated and non-heat-treated composites, while a decrease of 54.8% was observed on comparing the wear rate of heat-treated alloy and composite at optimum parameters. The wear rate increased with applied load, decreased initially and then increased with sliding distance and sliding velocity. Analysis of variance predicted applied load as the major influential parameter, followed by sliding distance and sliding velocity. Worn surface analysis revealed increase in delamination along with mild to severe wear transition with increase in applied load, and the formation of a mechanically mixed layer with increase in sliding velocity. This composite having high wear rate and hardness could be utilized for automotive load bearings, cylinder liners and brake drum applications.

**Keywords** Functionally graded materials · Heat treatment · Copper · Adhesive wear · Taguchi · ANOVA

## 1 Introduction

As commercial copper–nickel alloys have superior thermal, corrosion and chemical characteristics [1], industries resort to widening their application scope by improving their poor mechanical and tribological aspects [2]. This is done through two methods: one, by incorporating a hard secondary phase; and two, by age hardening mechanism. Introducing hard secondary phases, i.e. ceramic reinforcements such as silicon carbide (SiC) and boron carbide (B<sub>4</sub>C) improves the tensile strength, wear resistance, creep and fatigue resistance of the composite, but compromises the toughness and ductile characteristics of pure copper [3, 4]. The secondary method, i.e. the heat treatment process not only improves the toughness of the material, but also improves the machinability and formability and helps in restoring the ductility of the material after a cold working process [5]. By varying the processing parameters (ageing temperature and ageing time), an optimum combination can be achieved where improved mechanical and tribological characteristics are attained without any reduction in the toughness and ductility characteristics [6]. Functionally graded (FG) metal matrix composites offer improved location-specific material characteristics suitable for certain engineering applications requiring enhanced gradient properties along the surface or core [7]. Centrifugal casting is chosen as the primary fabrication route by many researchers, as it is the simplest and cost-effective method out of various processing methods for FG materials. The mechanical and tribological aspects of

✉ N. Radhika  
n\_radhika1@cb.amrita.edu

<sup>1</sup> Department of Mechanical Engineering, Amrita School of Engineering, Amrita Vishwa Vidyapeetham, Coimbatore, India

centrifugally cast FG composites have been studied extensively, highlighting the improved hardness and wear resistance [8]. Increasing the volume fraction of reinforcement particles up to 60% improves the mechanical and tribological characteristics of copper composites [9]. Titanium carbide (TiC), a non-oxide ceramic material, is chosen as reinforcement material owing to its high hardness, high grain refining effect, high modulus, and high chemical stability [10–13]. As there is sufficient literature available on the hard secondary phase method, our focus mainly is on the age hardening method. On comparing the characteristics of the heat-treated composite and alloy with the non-treated composite and alloy, increases in strength, hardness and wear resistance are the primary observations made, mainly due to the low propensity for crack propagation and nucleation [14]. Enhanced fracture toughness of the composite is mainly due to fine particles precipitating in the matrix structure of the specimen aged at 170 °C, while low fracture toughness is observed for specimen heat treated at 270 °C, mainly due to the dendritic microstructure [15]. Improvement in wear characteristics is observed when the cast specimen and T6 heat-treated composite specimens are abrasive wear tested, owing to the formation of precipitates during the ageing process. The applied load is predicted to have the highest influence on the wear rate of heat-treated FG copper composites, while sliding distance displayed minimum significance on the wear rate [16]. Statistical analysis performed on stir-cast Cu–Sn–Ni/Si<sub>3</sub>N<sub>4</sub> composites reveals that applied load and the interaction between applied load and sliding distance have prime influence on the wear rate [17].

In view of the above literature, the present study aims to bridge the literature gap between sliding wear analysis and heat-treated FG copper matrix composites. The hardness values of all heat-treated specimens are studied initially to obtain the optimum condition at which the specimen displays the highest hardness values. Further, the specimen having the highest hardness is then studied for its dry sliding wear behaviour under varying process parametric conditions. The results obtained are then systematically analysed using Taguchi's design of experiments (DOE) and analysis of variance (ANOVA) to understand the influence of the parametric conditions and to obtain an optimum processing condition at which the heat-treated specimen performs the best.

## 2 Synthesis of the FG Composite and Heat-Treatment Process

A two-step fabrication process was used to synthesize functionally graded (FG) copper composite of dimension  $\text{Ø}_{\text{out}} 100 \times \text{Ø}_{\text{in}} 70 \times 100 \text{ m}$ . The first step involved the

stir casting of copper alloyed with silicon (4 wt%) and nickel (11 wt%), and titanium carbide (10 wt%) particles of 10  $\mu\text{m}$  average particle size were added as reinforcement. The addition of alloying elements such as Ni to the base metal matrix enhanced the ultimate tensile strength as well as thermal stability, while adding Si enhanced the poor wettability and tribological characteristics of pure copper with TiC. The second step involved the centrifugal casting of the molten Cu–Ni–Si/TiC composite obtained from the electric resistance furnace operating at a temperature of 1060 °C. A steel die rotating at 1200 rpm was employed for producing a casting of dimension  $\text{Ø}_{\text{out}} 100 \times \text{Ø}_{\text{in}} 70 \times 100 \text{ mm}$ . Under the application of both centrifugal force and density variation, the low-density reinforcement particles (4.93 g/cc) segregated at the inner periphery making it a particle-rich region.

As the inner layer of the casting had a very rich concentration of TiC reinforcement particles, sample specimens were obtained from the inner zone for solution treatment. Solution treatment was performed at 850 °C for 1 h, followed by water quenching. These specimens were then subjected to different ageing conditions by varying the ageing temperature (450, 500, and 550 °C) and holding time (4, 6 and 8 h). The ageing temperature and holding time at which the specimen displayed the maximum hardness values were considered as the optimum conditions and the specimen at that condition was further experimented upon.

## 3 Experimental Procedures

This section deals with the detailed explanation about the micro-hardness, metallurgical, XRD and sliding wear tests performed.

### 3.1 Micro-Hardness Test

The non-heat-treated and heat-treated sample specimens were tested for their micro-hardness using Vickers Hardness Tester (Mitutoyo 201-101 E; Kawasaki, Japan), following the American Society for Testing and Materials (ASTM) E92 standard. A test specimen was kept on the table and a test force of 100 gf was applied for 15 s to produce an indentation on the specimen surface. The diagonal lengths of the indentation were measured, and the hardness value was noted. The average of the total measured values is taken as the micro-hardness of the specimen.

### 3.2 Metallurgical Test

The metallographic study of sample specimen which displayed the highest hardness was conducted using Zeiss Axiovert 25 (Inverted Microscope Model EP-IMET 3). A specimen of dimension  $10 \times 10 \times 20$  mm, cut from the heat-treated FG sample, was finisher polished to remove burr defects and provide flatness to the surface. The specimen was then successively polished using emery papers (400, 600, 800 and 1000 grit size) and velvet polished (disk polisher equipped with alumina solution) to obtain a clear, high reflective surface without any scratches. An etchant was applied on the specimen surface to selectively attack the features of the structures and, then, the microstructure of the specimen was observed.

### 3.3 XRD Analysis

The heat-treated sample specimen having the highest hardness value was analysed using X-ray diffraction analysis to understand the phase formation and characteristics of the FG composite. An X-ray diffractometer (Bruker, D8 Advance, Germany) with Cu-K $\alpha$  radiation, operated at 40 kV and 40 mA, was employed to obtain the diffraction data of the sample specimen. A scanning speed of  $5^\circ/\text{min}$  and a scan step of  $0.03^\circ$  were selected. The data obtained were analysed and matched to identify the phases formed at the copper matrix–reinforcement interface.

### 3.4 Wear Test and Analysis

To understand how heat treatment and reinforcement introduction affected the wear characteristics, samples obtained from the inner periphery of the heat-treated composite ( $550^\circ\text{C}/6\text{ h}$ ) and heat-treated alloy were studied using experiments performed on a DUCOM pin-on-disk tribometer. A constant track diameter of 80 mm was set on the track scale for all experiments. Before each experiment, the counterface (hardened steel disk, 10 mm thickness, HRC 57) was polished using emery papers of grit size 600 and 800 to ensure full specimen patch contact. Rectangular specimens of dimension  $10 \times 10$  mm were machined as per ASTM G99 standard in such a way that the inner layer of the composite acted as the face of the pin sliding against the counterface. The height of the specimen was increased by fixing 30 mm hollow stainless steel pipe on the other face of the pin through cold setting. Taguchi's DOE was preferred as the optimum method to conduct the adhesive wear experiments. The number of experiments to be conducted was decided based on the L27 orthogonal array. The applied load (10, 20, 30 N), sliding distance (500, 1000, 1500 m), and sliding velocity (1, 2, 3 m/s) were chosen as the processing parameters. An electronic weighing balance

was used to weigh the pins prior to and after each experiment. Each specimen was cleaned thoroughly using acetone solution. The wear rate calculated from the weight loss of the specimen was obtained and the obtained results were tabulated and analysed using MINITAB 18 statistical software.

## 4 Results and Discussions

X-ray diffraction (XRD) analysis, Vicker's hardness test, microstructural evaluation, adhesive wear test, and worn surface analysis were conducted and their results are elaborated in the following sections.

### 4.1 Micro-Hardness Tests

Micro-hardness test performed on the non-heat-treated FG composite samples reveals high hardness (116 HV) at the inner periphery due to the high concentration of reinforcement particles, while the outer zone displays hardness values of 102 HV. Figure 1 illustrates the variation in hardness values from the outer periphery to the inner core layers of the FG composite before the solution and ageing treatment. The average Vicker's hardness value of each heat-treated sample is plotted (Fig. 2) as a function of ageing temperature and holding time at constant solutionizing conditions ( $850^\circ\text{C}/1\text{ h}$ ). Out of nine parametric combinations of heat treatment, the sample specimen aged

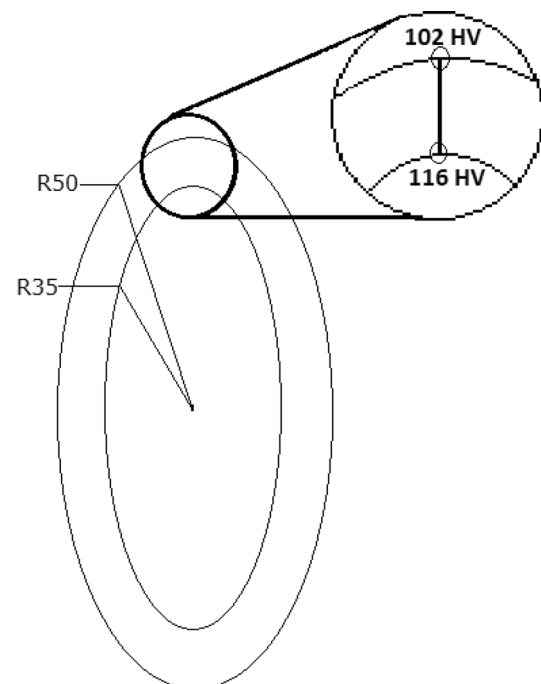
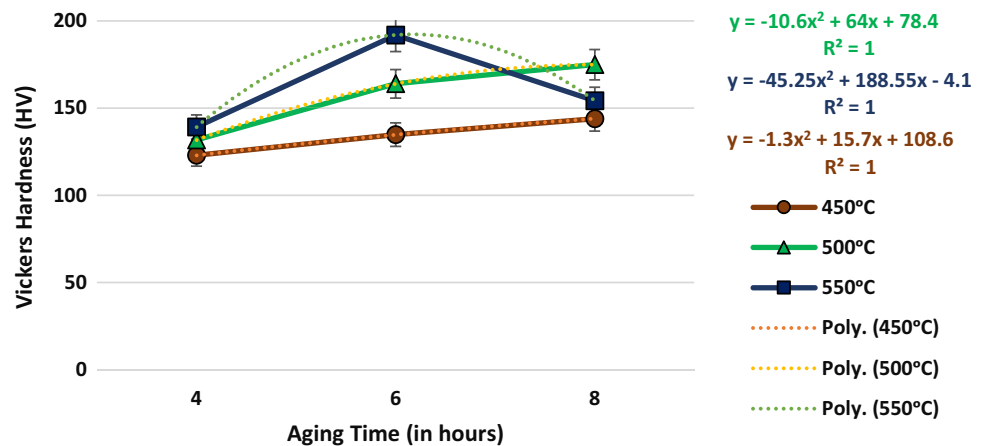


**Fig. 1** Hardness profile at as-cast condition

**Fig. 2** Variation in micro-hardness at heat-treated conditions



at 550 °C for 6 h displays the maximum hardness value of 192 HV. Employing artificial or natural ageing immediately after quenching increases the hardness substantially. This is mainly due to  $\alpha$ -phase copper and  $\text{CuNi}_2\text{Si}$  phase formation within the matrix structure. An increase in the rate of precipitation formation is observed with increase in ageing temperature and ageing time up to 500 °C. Prolonged ageing duration (up to 6 h) increases the formation of the precipitated phases, which in turn improves the hardness. On ageing beyond 6 h, structural coarsening is observed, due to which the strength and hardness decrease. From Fig. 2, an increasing hardness trend is observed for the specimen treated at 550 °C only up to an ageing time of 6 h, beyond which a steady decrease in hardness is observed, owing to the dissolution of the precipitate above the critical temperature.

#### 4.2 Metallurgical Investigation

Figure 3a represents an optical micrograph of the inner layer of the FG Cu–Ni–Si/TiC composite microstructure at as-cast condition, while Fig. 3b represents an optical micrograph of the FG Cu–Ni–Si/TiC composite microstructure heat treated at 550 °C for 6 h. From Fig. 3a, it is clearly confirmed that the inner layers of the composite contain a very large concentration of TiC reinforcement particles, mainly due to the high boundary energy during solidification and the centrifugal force action making the particles move radially inward and accumulate at the grain boundaries. On analysing the micrographs using ImageJ software, it is confirmed that around 20–30 vol% of TiC particles are present on the surface of the sample specimen making it a particle-enriched specimen. Figure 3b shows that some amount of precipitation is observed in the microstructure, as the surface reveals a large amount of continuous white phases along the grain boundaries which improves the strengthening effect. The interface behaviour of matrix and reinforcement particle is also crucial, as it

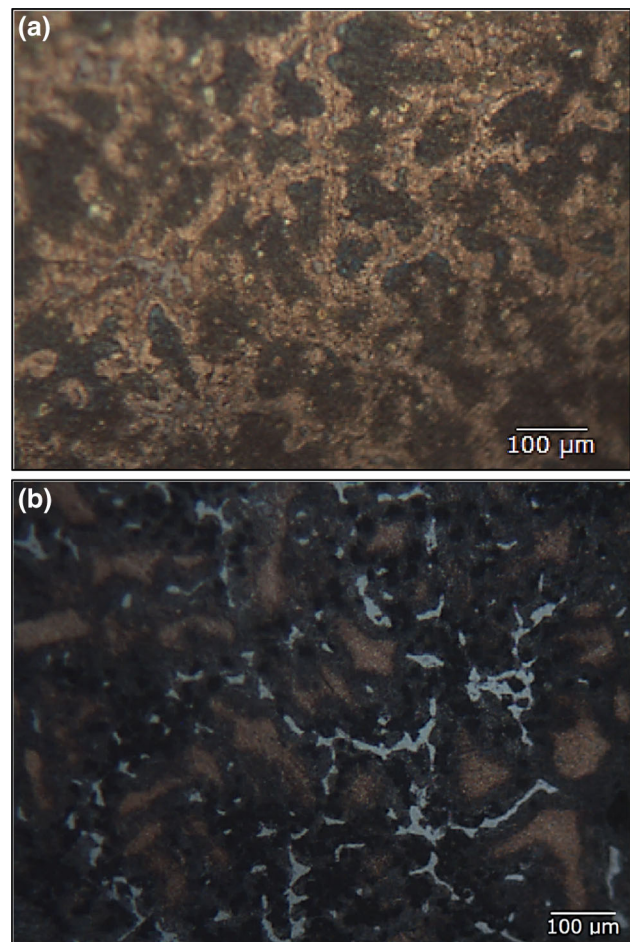


**Fig. 3** Metallographic structure of Cu–Ni–Si/TiC composite at (a) as-cast condition (b) 550°C/6h heat-treated condition

enhances the properties (physical and mechanical) of the composite. A large concentration of TiC particles are focussed on the primary  $\alpha$ -grain boundaries and does not act as nucleation sites for primary- $\alpha$  grain, which have an average size close to 100  $\mu\text{m}$  [18]. It should be noted that

the number of pores present on the surface of the specimen is also minimum, highlighting the effect of heat treatment.

Figure 4 depicts the X-ray diffraction spectra of FG Cu–Ni–Si/TiC composite specimen heat treated at 550 °C for 6 h. Analysis confirms the formation of the CuNi<sub>2</sub>Si phase, which is in accordance with the literature [19]. Low peaks of TiC are also observed, which is confirmed using JCPDS card #65-8246. This confirms the presence of reinforcement particles in the composite matrix. A shift in the diffraction angle to higher angles is also observed. No other crystalline phases are detected within the sensitivity of the XRD device. High peaks of copper are also observed along with a shift in the diffraction angles to lower angles. This can be explained as being due to the formation of the CuNi<sub>2</sub>Si intermetallic phase which enhances the tribo-mechanical characteristics after heat treatment. The presence of both Cu and TiC peaks indicates that no reaction has occurred between the matrix and reinforcement to form additional phases,

### 4.3 Wear Test and Analysis

The “smaller-the-better” characteristics have been chosen for predicting the minimum wear process parameter conditions. Table 1 shows the results of the wear test performed on samples prepared from the inner layers of heat-treated TiC-reinforced FG composite and heat-treated FG alloy. The process parameters are ranked based on the influence of the S/N ratio, obtained through Taguchi’s DOE technique. The delta value for each process parameter has been calculated based on the difference in the peak values and the ranking is made in decreasing order. Tables 2 and 3 represent the S/N ratio response tables for the composite and alloy, respectively. The applied load is the major parameter having primary influence on the applied wear rate, then on sliding distance and sliding velocity (Table 2). The last row of Table 2 indicates the

ranking of process parameters in the order they influence the S/N ratio.

### 4.4 Influence of Processing Parameters on Wear Rate

The S/N ratio plot (Fig. 5) illustrates the optimum level for individual parameters for the heat-treated FG composite and FG alloy, respectively, while the mean plot (Fig. 6) illustrates the wear behaviour trends for each level of the processing parameter for the composite and alloy, respectively. Analysing the S/N plots for both the composite and alloy reveals the optimum process parameter condition at which maximum wear resistance can be achieved. The optimum condition for heat-treated composite as obtained from the S/N plot is  $L = 10$  N,  $V = 2$  m/s and  $D = 1500$  m, while for heat-treated alloy the optimum parameter condition is  $L = 10$  N,  $V = 1$  m/s and  $D = 500$  m.

#### 4.4.1 Influence of the Applied Load

Figure 6a, d reveals an increasing trend in wear rate with increase in applied load for both the heat-treated FG composite and the heat-treated FG alloy, respectively, while keeping the sliding velocity and sliding distance constant at 2 m/s and 1000 m, respectively. At an applied load of 10 N, the contact stresses acting on the sliding pin are minimal. Hence, the material removal rate is low for both alloy and composite. The wear rate for heat-treated composite is minimal due to the presence of both TiC reinforcement particles and the precipitates contributing as resistance towards material removal, whereas for the heat-treated alloy, the wear resistance is mainly due to the precipitates inhibiting the movement of dislocations or defects in the crystal lattice. As the load applied externally increases from 10 to 20 N, the contact stresses acting at the pin–disk interface increases, leading to breakage of the strong intermolecular bonds causing plastic deformation of pin material coming in continuous contact with the sliding disk. Increase in temperature at the pin–sliding disk interface is also observed which aids in the plastic deformation of the material, thereby increasing the wear rate [20]. At high applied load (30 N), the highest material removal is observed mainly due to the high contact stresses aiding in the rise in temperature, which leads to localized pin material adhesion onto the sliding disk [21]. The wear rate of the composite is observed to increase continuously with increase in contact pressure, which is consistent with Archard’s law. On comparing both alloy and composite, a better wear resistance is observed for the heat-treated FG composite due to the presence of the added reinforcement particles.

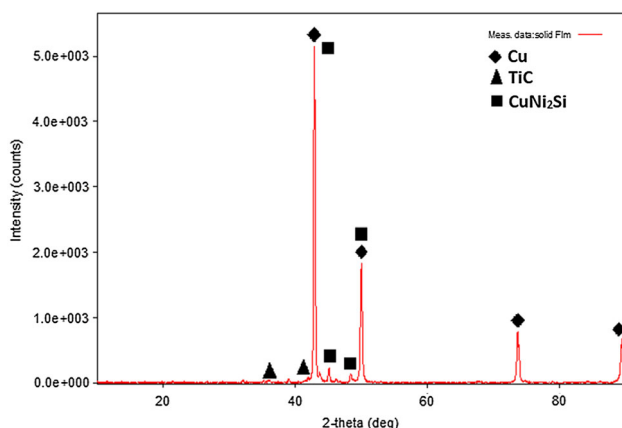


**Fig. 4** X-ray diffractogram of the 550 °C/6 h heat-treated sample

**Table 1** Wear results of A: heat-treated composite; B: heat-treated FG alloy

Applied load (N)	Sliding velocity (m/s)	Sliding distance (m)	Wear rate of A (mm <sup>3</sup> /m)	S/N ratio of A (dB)	Wear rate of B (mm <sup>3</sup> /m)	S/N ratio of B (dB)
10	1	500	0.00047	66.5580	0.00104	59.6538
10	2	500	0.00023	72.7654	0.00130	57.7033
10	3	500	0.00031	70.1728	0.00147	56.6615
10	1	1000	0.00070	63.0980	0.00117	58.6264
10	2	1000	0.00023	72.7654	0.00140	57.0692
10	3	1000	0.00023	72.7654	0.00164	55.7102
10	1	1500	0.00117	58.6363	0.00136	57.3420
10	2	1500	0.00164	55.7031	0.00154	56.2552
10	3	1500	0.00115	58.8239	0.00177	55.0438
20	1	500	0.00317	49.9816	0.00136	57.3377
20	2	500	0.00257	51.8013	0.00151	56.4205
20	3	500	0.00130	57.7211	0.00166	55.6013
20	1	1000	0.00287	50.8454	0.00158	56.0012
20	2	1000	0.00093	60.6303	0.00169	55.4217
20	3	1000	0.00140	57.0774	0.00187	54.5446
20	1	1500	0.00164	55.7031	0.00174	55.2090
20	2	1500	0.00070	63.0980	0.00191	54.3975
20	3	1500	0.00187	54.5632	0.00201	53.9447
30	1	500	0.00746	42.5452	0.00173	55.2290
30	2	500	0.00348	49.1634	0.00200	53.9968
30	3	500	0.00086	61.3100	0.00224	52.9821
30	1	1000	0.00572	44.8566	0.00198	54.0521
30	2	1000	0.00234	52.6157	0.00218	53.2495
30	3	1000	0.00055	65.1927	0.00243	52.2736
30	1	1500	0.00445	47.0348	0.00215	53.3701
30	2	1500	0.00218	53.2349	0.00238	52.4587
30	3	1500	0.00055	65.1927	0.00266	51.5089

**Table 2** S/N ratio response for the FG composite

Level	Applied load (N)	Sliding velocity (m/s)	Sliding distance (m)
1	65.70	58.00	53.25
2	55.71	59.98	59.09
3	53.46	56.89	62.54
Delta	12.24	3.10	9.28
Rank	1	3	2

#### 4.4.2 Influence of Sliding Velocity

On analysing the trends observed in Fig. 6b, e while maintaining applied load as 20 N and sliding distance as 1000 m, a steep decrease in wear rate is observed for the heat-treated composite (Fig. 5b), while a linearly increasing trend is observed for the heat-treated alloy (Fig. 5e). At initial velocity conditions (1 m/s), the heat-treated

composite has high wear resistance values than the alloy due to the presence of both reinforcement particles and precipitates acting as inhibitors to dislocation motion, while for heat-treated alloy, the presence of the precipitates offers very little wear resistance when compared to the heat-treated composite, leading to a higher material removal rate than the alloy. The high wear rate at low sliding velocity condition is mainly due to the high

**Table 3** S/N ratio response for the FG alloy

Level	Applied load (N)	Sliding velocity (m/s)	Sliding distance (m)
1	57.12	56.31	56.18
2	55.43	55.22	55.22
3	53.24	54.25	54.39
Delta	3.88	2.06	1.78
Rank	1	2	3

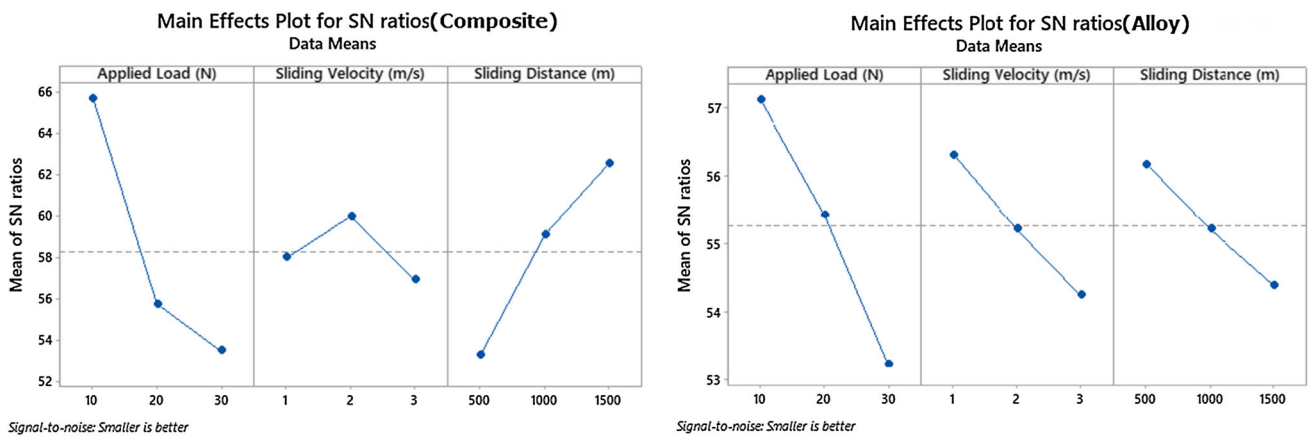


**Fig. 5** Main effects plot for S/N ratios—wear rate

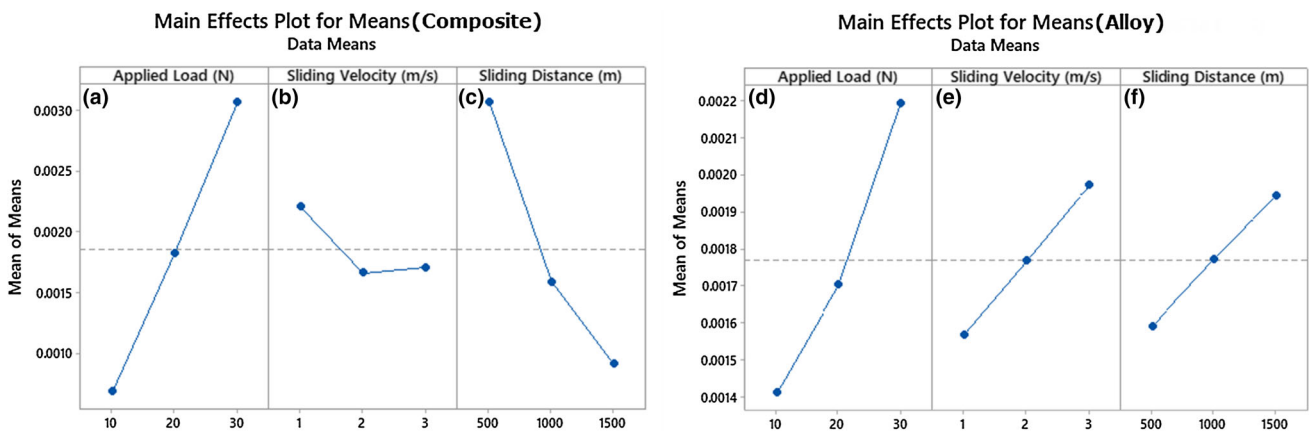


**Fig. 6** Main effects plot—wear rate

interaction period between the sliding pin and counterface. This leads to the building up of contact stresses at the point of contact, leading to high material removal rate. As the sliding velocity increases from 1 to 2 m/s, a slight decrease in wear rate is observed for the composite with increase in the sliding velocity, while an increasing trend is observed for the alloy. For the composite, a decrease in the wear rate trend is mainly due to the formation of a thin oxide layer on the surface of the pin, known as the mechanically mixed layer (MML) [22, 23]. This layer is formed due to the mixing of the wear debris produced by the micro-cutting

effect with the metal oxides, acting as a lubricating layer reducing friction and thus reducing the material removal rate for the composite. For the alloy, the precipitates which initially provide resistance to deformation lose its strength, thus leading to a high material removal rate. At high velocity (3 m/s), this tribolayer formed on the surface on the composite pin becomes unstable, leading to the peeling off of the layer and thus to a slight increase in the wear rate. This transition of wear rate is mainly due to a combination of high applied load and high sliding velocity exerting very high pressure on the disk and causing specimen material

loss [24]. The fresh layer of material beneath the tribolayer is exposed, which increases the wear rate by producing a pitting phenomenon. For heat-treated alloy, the wear rate is found to increase due to decrease in the strength and hardness which occurs due to a combination of high speed and high applied load. On comparing wear rate of both the alloy and composite samples, it is evident that heat-treated FG composite performs exceedingly well due to the added effect of reinforcement and precipitates, while for the alloy, the presence of precipitates does not act much as a resistance to the material removal rate.

#### 4.4.3 Influence of Sliding Distance

Keeping applied load as 20 N and sliding velocity as 2 m/s respectively, a decreasing trend in wear rate is observed for the heat-treated composite (Fig. 6c), while an increasing trend is observed for the heat-treated alloy as the sliding distance increases up to 1500 m (Fig. 6f). Initially at low sliding distance (500 m), a high wear rate is observed owing to the sharp asperities present on the composite surface. These protrusions reduce the area of contact between the sliding disk and the pin specimen, which increase the wear rate. For alloy, initial wear resistance is offered due to the formation of the  $\text{CuNi}_2\text{Si}$  phases which act as inhibitors to the deformation action. As sliding distance increases from 500 to 1500 m, a steep decrease in the wear rate is observed for the composite, owing to the hard asperities getting compacted between the sliding surfaces. These asperities which are initially in contact with the sliding counterface become blunt and smoothed, thereby increasing the area of contact between the sliding surfaces [25, 26]. For the alloy, the resistance offered by the precipitates becomes weak, leading to an increase in the material removal rate. The influence of heat treatment and ageing process on the mechanical and tribological properties has been elucidated in the previous sections. The strong interfacial bonding between the matrix and the reinforcement particles and also the formation of the  $\text{CuNi}_2\text{Si}$  phase aid in the reduction of the wear rate of the composite. The reinforcement particles are strongly encapsulated by the copper matrix, hence protecting the pin contact surface during sliding and reducing the wear rate.

#### 4.5 Analysis of Variance (ANOVA)

Statistical analysis performed through ANOVA confirms that the applied load has the highest percentage of contribution among all processing parameters influencing the wear rate of the heat-treated composite and alloy. The results obtained from ANOVA are depicted in Tables 4 and 5, respectively. From Table 4, it is verified that the applied load (32.10%) has the most influence on the wear rate of

the composite, followed by sliding distance (27.16%) and then sliding velocity with the least influence (2.47%). For the alloy, the applied load has the highest influence (60%), followed by the sliding velocity (20%) and sliding distance (20%). It is noted that out of all interactions, the interaction between the applied load and the sliding distance has the highest dominance (27.16%) for the composite. It should be noted that the observations and inferences made are relevant and unique to this specimen. The sliding distance and sliding velocity influence may vary depending on the material structure and compositions, thereby changing the rank of influence. Even then, applied load is concluded to be the most important process parameter for most copper matrix composites.

#### 4.6 Regression Analysis and Confirmation of Experiments

This can be defined as a statistical process which correlates various processing parameters such as load ( $L$ ), distance ( $D$ ), and velocity ( $V$ ) and their interactions mathematically, to compute the wear rate. The equation obtained for the heat-treated composite is as follows:

$$\begin{aligned} \text{Wear rate}(\text{mm}^3/\text{m}) = & -0.00375 + 0.000496L \\ & + 0.000189V + 0.000001D, \\ & - 0.000063L * V + 0.000001V * D \end{aligned}$$

and for heat-treated alloy the equation obtained is as follows:

$$\begin{aligned} \text{Wear rate}(\text{mm}^3/\text{m}) = & 0.000327 + 0.000032L \\ & + 0.000214V + 0.000000D \\ & + 0.000001L * V. \end{aligned}$$

It is confirmed that the applied load is the most important parameter of all process parameters for both the composite and alloy, as it has the highest influence on the wear rate regression equation. Sliding distance has the least influence of all parameters, due to the low coefficient value. Confirmation experiments are the final step in validating the regression equation. Table 6 represents the random chosen parametric combinations for the confirmation experiments within the range of parametric values for both heat-treated composite and alloy. Tables 7 and 8 display the results of the confirmation experiments and comparative analysis between the experimental values and the computed values from the regression equation model for the heat-treated composite and heat-treated alloy, respectively.

Analysis of confirmation experiments performed for the heat-treated composite reveals the regression model wear rate varying from experimental wear rate by an error percentage between 2.65 and 7.48%, while for the heat-treated



**Table 4** ANOVA analysis results for the heat-treated composite

Source	DoF	Adj S.S	Adj M.S	F-value	P value	P (%)
Applied load	2	0.000026	0.000013	54.60	0.000	32.10
Sliding velocity	2	0.000002	0.000001	3.50	0.081	2.47
Sliding distance	2	0.000022	0.000011	46.80	0.000	27.16
Applied load × sliding velocity	4	0.000005	0.000001	5.66	0.018	6.17
Applied load × sliding distance	4	0.000022	0.000006	23.65	0.000	27.16
Sliding velocity × sliding distance	4	0.000002	0.000001	2.66	0.111	2.47
Error	8	0.000002	0.000000			2.47
Total	26	0.000081				100

**Table 5** ANOVA analysis results for the heat-treated alloy

Source	DoF	Adj S.S	Adj M.S	F-value	P value	P (%)
Applied load	2	0.000003	0.000001	2622.98	0.000	60
Sliding velocity	2	0.000001	0.000000	684.04	0.000	20
Sliding distance	2	0.000001	0.000000	524.87	0.000	20
Applied load × sliding velocity	4	0.000000	0.000000	15.71	0.001	0
Applied load × sliding distance	4	0.000000	0.000000	5.84	0.017	0
Sliding velocity × sliding distance	4	0.000000	0.000000	0.95	0.485	0
Error	8	0.000000	0.000000			0.0
Total	26	0.000005				100

**Table 6** Chosen parametric combination for confirmation experiments

Experiment no.	Load ( <i>L</i> ), N	Velocity ( <i>V</i> ), m/s	Distance ( <i>D</i> )
1	13	1.4	600
2	19	2.3	900
3	24	2.8	1400

**Table 7** Confirmation experiment results for the heat-treated composite

Experiment no.	Exp. wear rate (mm <sup>3</sup> /m)	Reg. model wear rate (mm <sup>3</sup> /m)	% error
1	0.003345	0.003256	2.65
2	0.006578	0.006326	3.84
3	0.01056	0.00977	7.48

**Table 8** Confirmation experiment results for the heat-treated alloy

Experiment no.	Exp. wear rate (mm <sup>3</sup> /m)	Reg. model wear rate (mm <sup>3</sup> /m)	% error
1	0.003345	0.00373	4.87
2	0.006578	0.001378	6.31
3	0.01056	0.001699	3.54

alloy, the error percentage varies from 3.54 to 6.31%. Hence, it can be concluded that the regression wear rate model and the experimental wear rate are nearly similar with the least error, highlighting the suitability of the mathematical model for predicting the dry sliding behaviour of the composite.

#### 4.7 Worn Surface Analysis

The heat-treated composite sample specimens (550 °C/6 h) used for studying the wear rate of applied load (10 and 30 N), sliding distance (500 and 1500 m) and sliding velocity (1 and 3 m/s) have been analysed using scanning electron microscope (SEM) to obtain a clear view of the wear morphologies, which reveal features such as cracks, grooves and delamination. The worn surface morphologies observed are as depicted in Figs. 7, 8 and 9.

At low load (10 N), the worn surface exhibits the presence of shallow grooves and a large number of delaminations, along with small patches of worn out material, which confirms that wear progresses by a combination of adhesive and abrasive mode of wear mechanism. This is mainly due to the low contact stresses produced by the applied load and the wear resistance offered by the hard TiC particles. The adhesive wear component is confirmed by the presence of material patches and the abrasive wear component by the presence of a number of shallow grooves (Fig. 7a). At high load (30 N), a large number of deep grooves are observed on the material surface along with the growth of small cracks, revealing the transition from normal wear to severe wear. Surface peel offs and torn outs are observed at high contact pressures, leading to the formation of a large number of delaminations (Fig. 7b), which confirms the transition from oxidative and adhesive wear to delamination wear [27].

High material removal in the form of very high delamination and material pull-out are observed at low sliding distances of 500 m (Fig. 8a), owing to the plastic deformation caused due to the increased interaction between the sliding pin and the hardened steel counterface, which raises the temperature at the point of contact [28]. High material removal is also observed mainly due to the non-uniform wear mechanism observed at the interface. The material removed initially as debris gets rolled between the pin and the steel disk, causing continuous rotation of the wear material. This leads to the formation of continuous delamination on the specimen surface until it is torn off from the pin surface, thus increasing the material removal rate. Small traces of delamination along with the presence of wear debris are observed at higher sliding distances (1500 m), mainly due to the presence of MML formation on the pin surface. Under these conditions, a decrease in the material wear rate is observed (Fig. 8b).

A combination of heavy delamination along with agglomeration and clustering of wear debris is observed at initial sliding velocity (1 m/s). This is mainly due to the high interaction period and the contact stresses which build up at the interface. This leads to the increase in the material removal rate, as observed in Fig. 9a. On transition from 1 to 2 m/s, a glossy flake forms on the wear track owing to the mixing of wear debris produced due to the micro-cutting effect. An oxygen-rich layer called mechanically mixed layer (MML) [29, 30] is formed along with other metallic oxides which aids in reducing the friction at the interface and increases the wear resistance (Fig. 9b).

EDX analysis of the wear specimen heat treated at 550 °C/6 h (Fig. 10) confirms the presence of iron and oxygen on the worn surface, which is mainly due to the presence of various oxides along with picking up of iron from the counter-disk. The transfer of material occurring

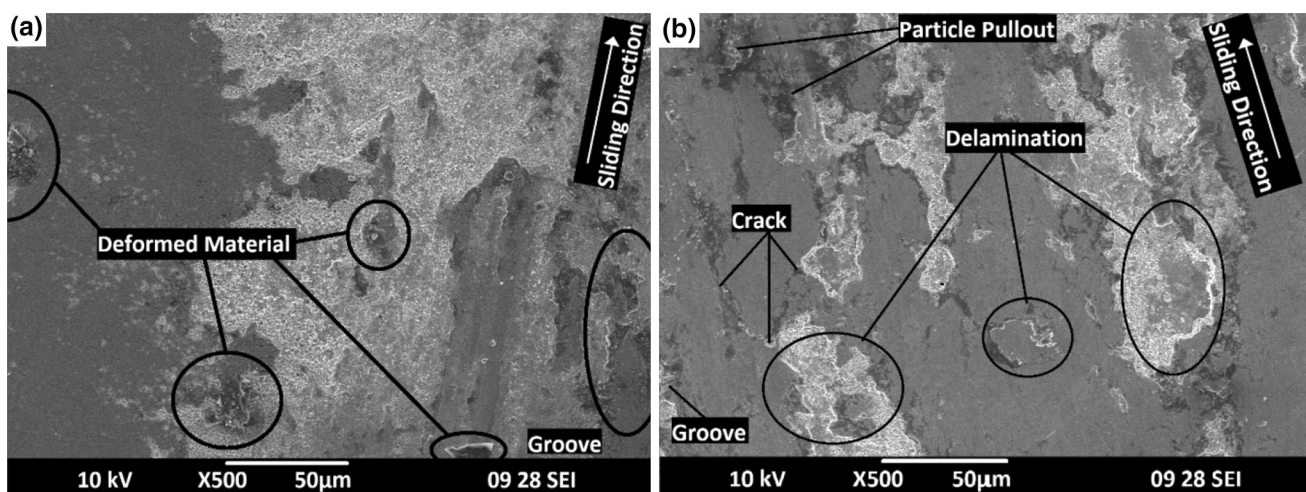


**Fig. 7** Worn surfaces of the FG composite at applied load: **a** 10 N, **b** 30 N

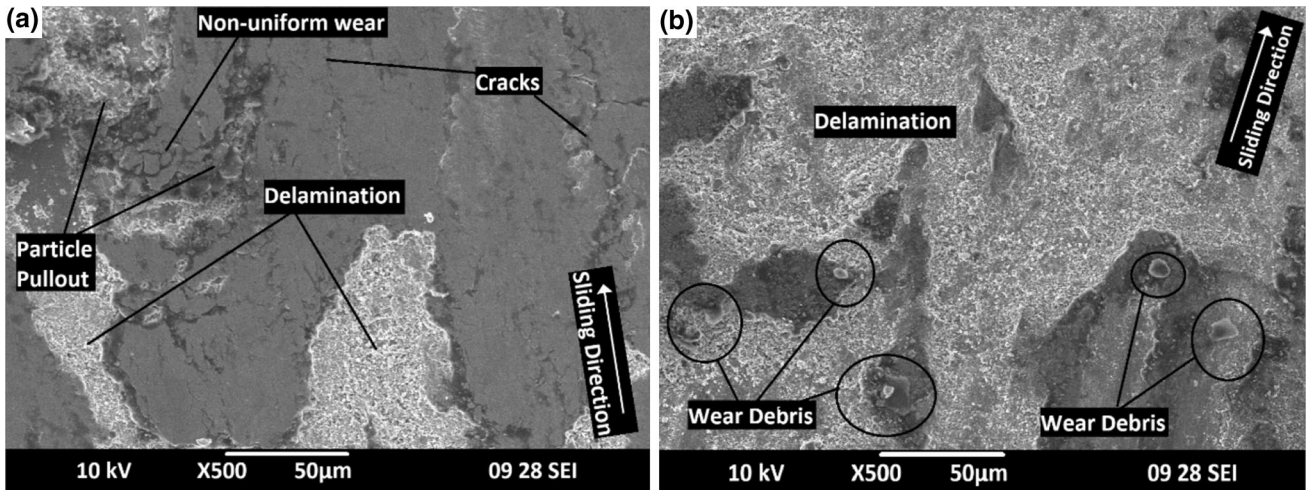


Fig. 8 Worn surfaces of the FG composite at sliding distance: a 500 m, b 1500 m

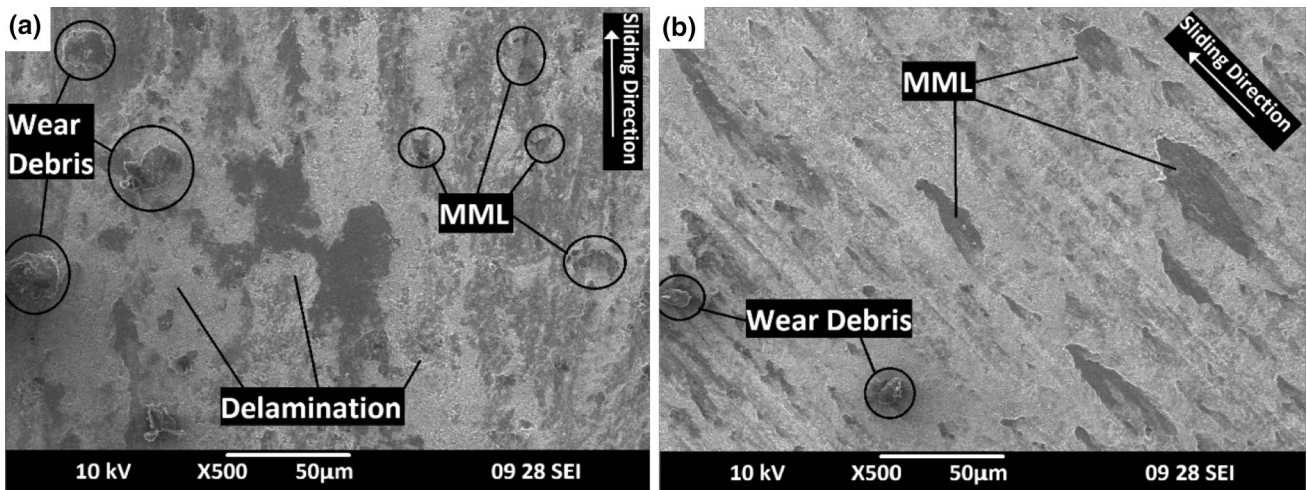


Fig. 9 Worn surfaces of the FG composite at sliding velocity a 1 m/s, b 3 m/s

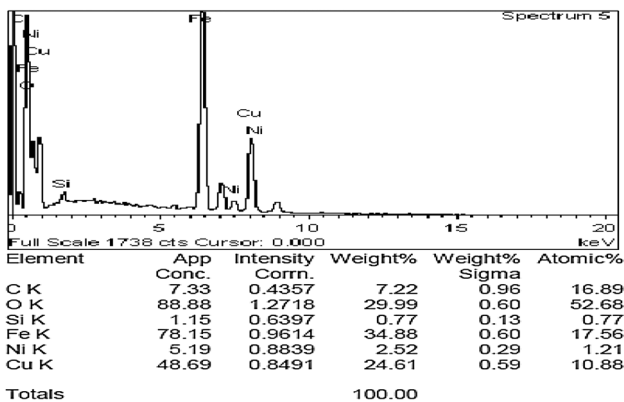
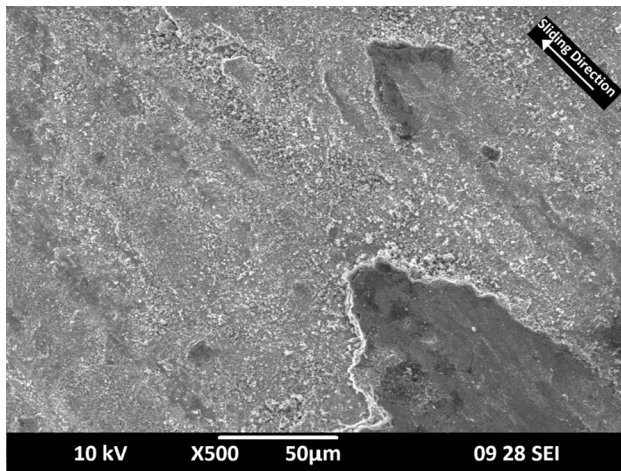


Fig. 10 EDX analysis of the 550 °C/6 h FG Cu/TiC specimen

between the counterface disk and the worn surface pin material indicates the resistance of a material to the wear action. The presence of oxygen promotes the metallic

oxide formation of aluminium, nickel, and iron, aiding in the tribolayer formation and thus reducing the wear rate.

Optimum wear processing conditions i.e.  $L = 10$  N,  $V = 2$  m/s and  $D = 1500$  m for minimum wear rate is obtained from Fig. 5. Metallographic surface image of pin material at the optimum parameter is depicted in Fig. 11. Minimal wear tracks, scratches and grooves are observed on the wear track. Peeling and accumulation of wear debris are not visible here as in other parametric conditions. Some amount of delamination is also observed on the wear surface, highlighting the superior particle matrix bond strength and the particle reorientation after heat treatment. The heat treatment process improves the boundary hardening, which results in decreasing the wear rate.



**Fig. 11** Worn surface morphology at optimum condition

## 5 Conclusion

The FG Cu–Ni–Si/TiC composite has been successfully fabricated through a two-step process, stir casting and then centrifugal casting. The specimens obtained from the inner layer of the composite are heat treated, under variable ageing temperature and ageing time.

- The composite specimen heat treated at 550 °C for 6 h displays the highest hardness (192 HV) among all heat-treated specimens. A 65% increase in hardness is observed on comparing the micro-hardness values of the heat-treated composite and the non-heat-treated composite.
- Dry sliding wear analysis is performed on the inner layer specimens obtained from the FG composite heat treated at 550 °C/6 h and from heat-treated alloy to predict the wear behaviour. For heat-treated composite, the wear rate increases with increase in the applied load. As sliding velocity increases, an initial decrease in wear rate is observed, which then increases with progression in parametric condition, while for sliding distance, a decrease in wear rate is observed with increasing parametric conditions. For the alloy, increasing wear trend is observed as applied load, sliding velocity and sliding distance increases. A 54.8% decrease in material removal rate is observed for the composite on comparing the wear rates of both heat-treated composite and alloy.
- Analysis of variance (ANOVA) and signal to noise ratio predict that the applied load has the highest influence of all processing parameters, followed by sliding distance and sliding velocity for both heat-treated composite and alloy. Mathematical regression model developed using MINITAB 17 is suitable to

predict the behaviour of dry sliding wear for the heat-treated composite and alloy with high accuracy.

- Metallographic analysis done on heat-treated composite wear samples reveals a transition in wear mechanism from mild wear to severe wear as the applied load increases. A formation of MML tribolayer is also observed with increase in sliding velocity.

This specimen, heat treated at 550 °C for 6 h, displays improved mechanical and sliding wear characteristics which can be employed for applications involving high tensile strength, hardness and wear resistance. This composite can be utilized for automotive load bearings, cylinder liners and brake drum where the high wear resistance of the inner layers is considered to be a good effect.

## References

1. Davis J R, *ASM Specialty Handbook: Copper and Copper Alloys*, ASM International, Materials Park (2001).
2. Zhuang J, Liu Y B, Cao Z Y, and Li Y Y, *Mater Trans* **51** (2010) 2311.
3. Shabani M, Paydar M H, Zamiri R, Goodarzi M, and Moshksar M M, *J Mater Res Technol* **5** (2016) 5.
4. Hong E, Kaplin B, You T, Suh M S, Kim Y S, and Choe H, *Wear* **270** (2011) 591.
5. Radhika N, and Subramanian R, *Int J Mater Res* **105** (2014) 875.
6. Mares M, *J Optoelectron Adv Mater* **3** (2001) 119.
7. Vieira A C, Sequeira P D, Gomes J R, and Rocha L A, *Wear* **267** (2009) 585.
8. Karun A S, Rajan T P D, Pillai U T S, Pai B C, Rajeev V R, and Farook A, *J Compos Mater* **50** (2016) 2255.
9. Sathiskumar R, Murugan N, Dinaharan I, and Vijay S J, *Mater Charact* **84**, (2013) 16.
10. Mohapatra S, Mishra D K, and Singh S K, *Powder Technol* **237**, (2013) 41.
11. Kennedy A R, Karantzalis A E, and Wyatt S M, *J Mater Sci* **34**, (1999) 933.
12. Sabbaghian M, Shamanian M, Akramifard H R, and Esmailzadeh M, *Ceram Int* **40** (2014) 12969.
13. Bourithis L, Milonas A, and Papadimitriou G D, *Surf Coat Technol* **165**, (2003) 286.
14. Sawla S, and Das S, *Wear* **257**, (2004) 555.
15. Hegde R, Sivaram N M, Ajaykumar B S, and Kirthan L J, *Int J Appl Eng Res* **12** (2017) 605.
16. Sam M, and Radhika N, *J Tribol* **140** (2018) 021606.
17. Nithesh R, Radhika N, and Sunder S S, *J Tribol* **139** (2017) 061603.
18. Karantzalis A E, Lekatou A, Georgatis E, Poulas V, and Mavros H, *J Mater Eng Perform* **19** (2010) 585.
19. Azzeddine H, Mehdi B, Hennem L, Thiaudière D, Alili B, Kawasaki M, Bradai D, and Langdon T G, *Mater Sci Eng A* **597** (2014)288.
20. Dwivedi D K, *Mater Des* **31** (2010) 2517.
21. Baradeswaran A, and Elaya Perumal A, *Compos Part B Eng* **54** (2013) 146.
22. Radhika N, and Subramanian R, *Tribol Mater Surf Interfaces* **7** (2013) 36.
23. Jo S K, Lee W J, Park Y H, and Park I M, *Tribol Lett* **45** (2012) 101.

24. Basavarajappa S, and Chandramohan G, *Mater Sci* **11** (2005) 253.
25. Zhang L, He X B, Qu X H, Duan B H, Lu X, and Qin M L, *Wear* **265** (2008) 1848.
26. Kaur K, Anant R, and Pandey O P, *Tribol Lett* **44** (2011) 41.
27. Mu Z, Geng H R, Li M M, Nie G L, and Leng J F, *Compos Part B Eng* **52** (2013) 51.
28. Jojith R, and Radhika N, *Part Sci Technol* **40** (2018) 292.
29. Sangaravadevel P, Natarajan N, and Krishnaraj V, *Appl Mech Mater* **852** (2016) 435.
30. Zhang G, and Schlarb A K, *Wear* **266** (2009) 745.